Electron Spin Echo Modulation and Nuclear Relaxation Studies of Staphylococcal Nuclease and Its Metal-Coordinating Mutants†

E. H. Serpersu,‡ J. McCracken,§ J. Peisach,§ and A. S. Mildvan*,‡

Department of Biological Chemistry, The Johns Hopkins University School of Medicine, 725 N. Wolfe Street, Baltimore, Maryland 21205, and Department of Molecular Pharmacology and Physiology and Biophysics, Albert Einstein College of Medicine, Yeshiva University, 1300 Morris Park Avenue, Bronx, New York 10461

Received April 26, 1988; Revised Manuscript Received June 27, 1988

ABSTRACT: Electron spin echo envelope modulation (ESEEM) spectroscopy has been applied to the determination of the number of water molecules coordinated to the metal in the binary complex of staphylococcal nuclease with Mn^{2+}, to the ternary enzyme–Mn^{2+}–3′,5′-pdTp complex, and to ternary complexes of a number of mutant enzymes in which metal-binding ligands have been individually altered. Quantitation of coordinated water is based on ESEEM spectral comparisons of Mn^{2+}–EDTA and Mn^{2+}–DTPA, which differ by a single inner sphere water, and with Mn^{2+}–$(H_2O)_6$. It was found that Mn^{2+} in the ternary complex of the wild-type enzyme has a single additional coordinated water, as compared to Mn^{2+} in the binary complex, confirming earlier findings based on T_1 measurements of bound water [Serpersu, E. H., Shortle, D. L., & Mildvan, A. S. (1987) *Biochemistry 26*, 1289–1300]. Ternary complexes of the mutant proteins D40E, D40G, and D21Y have the same number of water ligands as the ternary complex of the wild-type enzyme, while the D21E mutant has one less water ligand. In order to maintain octahedral coordination geometry, these findings require two additional ligands to Mn^{2+} from the protein in the binary complex of the wild-type enzyme, probably Glu 43 and Asp 19, and one additional ligand from the protein in the ternary D40G and D21E complexes. Other ESEEM studies of ternary Mn^{2+} complexes of wild-type, D21E, and D21Y mutants indicate the coordination by Mn^{2+} of a phosphate of 3′,5′-pdTp, as demonstrated by a ^{31}P contact interaction of 3.9 ± 0.3 MHz. Magnetic interaction of Mn^{2+} with ^{31}P could not be demonstrated with the D40G and D40E mutants, suggesting that metal–phosphate distances are greater in these mutants than in the wild-type protein. In a parallel NMR study of the paramagnetic effects of enzyme-bound Co^{2+} (which occupies the Mn^{2+} site on the enzyme) on the T_1 of ^{31}P from enzyme-bound 3′,5′-pdTp and 5′-TMP, it was found that metal to 5′-phosphate distances are 0.9–1.6 Å shorter in ternary complexes of the wild-type enzyme and of the D21E mutant than in ternary complexes of the D40G mutant. In all cases, the 5′-phosphate of pdTp is in the inner coordination sphere of Co^{2+} and the 3′-phosphate is predominantly in the second coordination sphere.

Staphylococcal nuclease, which catalyzes the hydrolysis of phosphodiester linkages found in DNA and RNA, requires Ca^{2+} for activity (Cuatrecasas et al., 1967). Certain other metals, such as Mn^{2+}, bind at the Ca^{2+} site, as shown by competition in kinetics and in binding studies and by parallel decreases in affinity for both Mn^{2+} and Ca^{2+} following the mutation of individual metal ligating residues (Serpersu et al., 1986, 1987). An X-ray crystal structure of the ternary complex of the enzyme with both Ca^{2+} and the substrate analogue 3′,5′-pdTp shows the environment of Ca^{2+} to have approximately octahedral coordination geometry, with the metal ligated to the carboxylates of Asp 21 and Asp 40, the amide carbonyl group of Thr 41, the 5′P of pdTp, and two water molecules. Asp 19 and Glu 43 are somewhat farther from the Ca^{2+}, in the second coordination sphere (Figure 1) (Cotton et al., 1979). A mechanism based on the X-ray structure and on kinetic and binding studies of mutant enzymes has been published (Serpersu et al., 1987). This mechanism involves nucleophilic attack on the coordinated phosphodiester phosphorus by an inner sphere water ligand to metal or by a second sphere water, subsequent to its deprotonation by Glu 43, which is thought to function as a general base (Cotton et al., 1979; Hibler et al., 1987; Mildvan et al., 1988).

With the D40E and D40G mutant enzymes, it was found that changes in the metal ligands at position 40 resulted in 12- and 30-fold decreases, respectively, in k_{cat}, presumably due to geometric and dynamic alterations at the reaction center. Changes at position 21 in the D21E and D21Y mutants resulted in 1500- and 29 000-fold decreases, respectively, in k_{cat}. The latter effect has been ascribed to occlusion of the binding site for the attacking deprotonated water molecule and the resulting loss of catalysis by approximation (Serpersu et al., 1987).

To examine in greater detail the structure of the mutant proteins having amino acid substitutions at the metal binding center, ESEEM[1] spectroscopy was used. This is an especially sensitive method for directly delineating the structure in the immediate environment of paramagnetic metal ions (Mims & Peisach, 1976, 1981; Peisach et al., 1979) without the limitations of NMR methods that are based on the effects of paramagnetic cations on longitudinal relaxation rates of water protons and of phosphorus nuclei. NMR methods require fast ligand exchange out of the paramagnetic enviroment (Mildvan & Gupta, 1978; Mildvan et al., 1980). With ESEEM spectroscopy we have determined differences in the number of

† This work was supported by National Institutes of Health Grants HL-13399 and RR-02583 (to J.P.) and DK-28616 (to A.S.M.).

‡ The Johns Hopkins University School of Medicine.

§ Albert Einstein College of Medicine.

[1] Abbreviations: Tris-HCl, tris(hydroxymethyl)aminomethane hydrochloride; TES, *N*-[tris(hydroxymethyl)methyl]-2-aminoethanesulfonic acid; ESEEM, electron spin echo envelope modulation; ESE, electron spin echo; DTPA, diethylenetriaminepentaacetic acid; 3′,5′-pdTp, thymidine 3′,5′-diphosphate.

0006-2960/88/0427-8034$01.50/0 © 1988 American Chemical Society

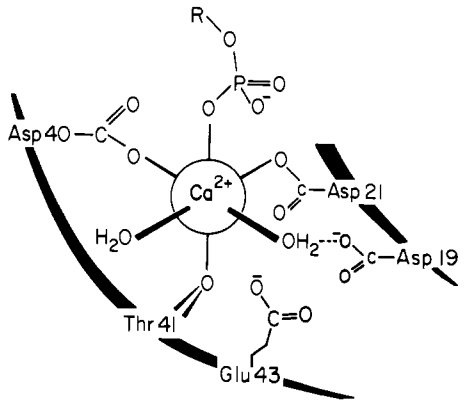

FIGURE 1: Active site of staphylococcal nuclease based on the 1.5-Å X-ray structure of the ternary enzyme–Ca^{2+}–pdTp complex (Cotton et al., 1979).

water ligands coordinated to enzyme-bound Mn^{2+} in both binary and ternary complexes of the wild-type enzyme and in ternary complexes of metal-ligating mutants. The results are in quantitative agreement with those based on paramagnetic effects of Mn^{2+} on water proton relaxation rates. Further, we are able to detect Mn^{2+}–phosphate bonding in some of the ternary complexes, as demonstrated by ^{31}P ESEEM where Fermi contact interactions were found similar to those observed by LoBrutto et al. (1986) for creatine kinase. The results obtained by electron spin echo methods with Mn^{2+} are in good agreement with parallel studies carried out with Co^{2+} using ^{31}P relaxation. Such agreement is expected in cases of fast ligand exchange. Preliminary reports of this work have been presented (Serpersu et al., 1988; McCracken et al., 1988).

Experimental Procedures

Materials

5′-TMP was purchased from Sigma, and 3′,5′-pdTp was obtained from P-L Biochemicals. Ultrapure hydrated $MnCl_2$ and $CoCl_2$ were from Johnson Matthey Chemicals. Before use, all buffer and nucleotide solutions were passed over Chelex 100 resin to remove trace metals. Salmon sperm DNA was obtained from Sigma. It was used in the enzyme assays following heat denaturation for 30 min at 100 °C and rapid cooling on ice (Cuatrecasas et al., 1967).

Methods

Isolation of the Enzymes. The preparation, isolation, genetic mapping, and sequence analysis of the staphylococcal nuclease genes of the wild-type and mutant enzymes used in this work have previously been described (Shortle & Lin, 1985). Purification to homogeneity of the wild-type and mutant staphylococcal nucleases from the engineered strain of *Escherichia coli* carrying the expression plasmid pFOG405 were performed as described previously (Serpersu et al., 1986). All mutant proteins are designated by their amino acid changes relative to the wild-type enzyme, using a three-symbol nomenclature in which the first letter designates the wild-type amino acid, the number designates the position of the amino acid, and the second letter designates the mutant amino acid substituted at this position.

Enzyme Assay. Staphylococcal nuclease activity was measured as described earlier (Serpersu et al., 1986, 1987) on the basis of the observation of the absorbance increase at 260 nm as DNA is hydrolyzed by the enzyme (Cuatrecasas et al., 1967). Typical assay mixtures contained saturating amounts of DNA (50–97.5 μg/mL) and Ca^{2+} (2–20 mM) in 40 mM Tris-HCl, pH 7.4, in a volume of 1.0 mL at indicated temperatures with and without 50% (v/v) ethylene glycol. To this mixture was added either 0.05–0.19 μg of wild-type enzyme or 1.4–2.8 μg of D40G, 0.4–0.75 μg of D40E, 17.5–21.0 μg of D21E, or 1.97–4.87 μg of T41P to start the reaction. Prior to their addition to the assay mixture, the enzymes were preincubated for 10 min with and without 50% (v/v) ethylene glycol. Velocity was determined from the linear portions of a plot of the change in absorbancy per minute per microgram of enzyme. Enzymatic activities were linear with the amount of protein used in the assays.

In kinetic experiments with Co^{2+} used as inhibitor, the assay mixture contained 49–70 μg of DNA, six concentrations of $CaCl_2$ ranging from 0.2 to 5.0 mM, and four concentrations of $CoCl_2$ ranging from 0 to 1.45 mM, in 40 mM Na TES, pH 7.4, in a volume of 1.0 mL at 24 ± 1 °C. The reaction was started by the addition of either 0.1 μg of wild-type enzyme or 1.6 μg of D40G or 21 μg of D21E to the reaction mixture. Tris buffer was not used in these studies because it is known to bind Co^{2+} (Hall et al., 1962). TES, which has a low affinity for Co^{2+}, was used instead, as well as for magnetic resonance experiments. In kinetic experiments, free Co^{2+} concentrations were estimated by assuming similar binding of Co^{2+} and Mn^{2+} to DNA (Hanlon et al., 1978), using the dissociation constant (68 μM) and stoichiometry (0.38 ± 0.04 site/DNA phosphorus) as was found for Mn^{2+} (Slater et al., 1972). Because the concentration of Co^{2+} exceeded the concentration of binding sites on DNA by at least an order of magnitude, the results are not very sensitive to the value of this dissociation constant. Protein concentrations were determined from the absorbance at 280 nm by using $\epsilon_{1cm}^{0.1\%} = 0.93$ with the exception of the D21Y mutant for which, because of the altered tyrosine content, the Bradford method (Bradford, 1976) was used instead with the wild-type enzyme as standard (Serpersu et al., 1987).

Binding Studies. The dissociation constants of Co^{2+} from the binary Co^{2+}–5′-TMP and Co^{2+}–3′,5′-pdTp complexes and from the ternary enzyme–Co^{2+}–nucleotide complexes were determined by competition with Mn^{2+}. EPR spectroscopy was used as an analytical tool to determine the concentrations of free Mn^{2+}. Measured dissociation constants of Mn^{2+} from binary and ternary complexes (Serpersu et al., 1987) were then used to calculate the concentrations of residual free nucleotide or enzyme–nucleotide complexes following the displacement of Mn^{2+} by Co^{2+}. In this way the concentrations of bound Co^{2+} and the dissociation constants of Co^{2+} were determined. In addition to EPR, measurements of $1/T_{1P}$ of water protons were also used with most of the ternary complexes to independently determine the dissociation constants of Co^{2+} from the concentration of free Co^{2+} necessary to displace half of the bound Mn^{2+}. The values of the dissociation constants obtained by both methods were in reasonable agreement, as indicated by the small errors in Table III.

Electron Spin Echo Envelope Modulation (ESEEM). Measurements were made at liquid helium temperatures and at X-band frequencies (~9.3 GHz) with a pulsed EPR apparatus described elsewhere (McCracken et al., 1987). ESEEM data were obtained by both the two-pulse and three-pulse or stimulated echo methods, as previously described (Peisach et al., 1979). To obtain a spectrum in the frequency domain, the echo envelopes, normalized to the intensity of the Mn^{2+} signal, were Fourier transformed by using the dead-time reconstruction procedure described by Mims (1984).

Two identical sets of samples were prepared, one in ^2H_2O and a second in H_2O. The ^2H_2O samples contained enzyme, buffer, and pdTp that had been deuteriated by lyophilization from ^2H_2O three times. The H_2O samples were lyophilized

and redissolved in H_2O. A concentrated stock solution of $MnCl_2$ in H_2O was diluted 100-fold into ^2H_2O for use with the samples prepared in ^2H_2O. Samples of ternary enzyme–Mn^{2+}–pdTp complexes in 40 mM Tris-HCl, pH 7.4, contained equimolar concentrations of enzyme and pdTp adjusted to give 1.0 mM bound Mn^{2+} and 0.040 mM free Mn^{2+} in each, as calculated from the known dissociation constants (K_A') of Mn^{2+} from these complexes (Serpersu et al., 1987). Samples of wild-type enzyme contained 3.22 mM protein and 0.33 mM Mn^{2+} to give the same concentration of free Mn^{2+} as the samples containing the ternary complexes. In each case, a 200-μL sample was used for ESEEM studies. A parallel series of samples diluted 1:1 (v/v) in ethylene glycol was also prepared. The use of ethylene glycol improved the signal/noise ratio of the ESEEM measurements but did not otherwise quantitatively alter the ESEEM data.

The model compounds Mn^{2+}–EDTA and Mn^{2+}–DTPA, each 1 mM, were prepared with a slight excess of chelator in ^2H_2O and in H_2O. These were prepared in 40 mM Tris-HCl, pH 7.4, which also contained 1:1 (v/v) ethylene glycol as described above.

Water Proton Relaxation Rate Measurements. The correlation times τ_c for the electron nuclear dipolar interaction in the ternary enzyme–Co^{2+}–nucleotide complexes were determined by studying the frequency dependence of $1/T_{1P}$ of water protons at 15, 24.3, 42, and 59.8 MHz on a Seimco pulsed NMR spectrometer equipped with a variable-frequency probe, at 250 MHz on a Bruker WM250 spectrometer, and at 360 MHz on a Bruker AM360 spectrometer by inversion recovery as previously described (Serpersu et al., 1986, 1987). Evaluation of τ_c from the frequency-dependent $1/fT_{1P}$ values was done as described earlier (Mildvan & Gupta, 1978; Mildvan et al., 1980). Samples contained 40 mM TES, pH 7.4, 0.81 mM $CoCl_2$, and equimolar concentrations of enzyme and either TMP or pdTp such that at least 66% of the Co^{2+} was bound in the respective ternary enzyme–Co^{2+}–nucleotide complexes. Wild-type enzyme and D21E were present at 0.96 mM, with equimolar TMP or pdTp. D40G concentrations were 1.69 and 1.10 mM with equimolar TMP and pdTp, respectively. The observed relaxation rates were corrected for the paramagnetic effects of free Co^{2+} in each system.

^{31}P Relaxation Rate Measurements. To determine the paramagnetic effects of Co^{2+} on the relaxation rates of the phosphorus nuclei of enzyme-bound 5′-TMP and 3′,5′-pdTp, 2.0-mL samples were prepared. These contained 10 mM TES, pH 7.4, 28 mM NaCl, 20% ^2H_2O for field/frequency locking, and appropriate concentrations of enzymes and TMP, such that in each case at least 95% of the enzyme was bound to nucleotide. Thus, the solutions contained 0.2 mM wild-type enzyme with 4.15 mM 5′-TMP, 0.4 mM D40G with 5.55 mM 5′-TMP, or 0.39 mM D21E with 4.88 mM 5′-TMP. The solutions were titrated with $CoCl_2$, measuring $1/T_1$ and $1/T_2$. At the end of the titrations, 3′,5′-pdTp was added stepwise to the samples, causing the complete removal of the observed paramagnetic effects of Co^{2+} on $1/T_1$ and $1/T_2$ of the phosphorus of TMP, indicating the total displacement of TMP from the ternary enzyme–Co^{2+}–TMP complexes by the tighter binding pdTp. This also showed that outer-sphere contributions to the observed ^{31}P relaxation rates were negligible. The samples in which all of the TMP had been displaced from the ternary complexes by pdTp contained 3.63 mM pdTp with the wild-type enzyme, 4.74 mM pdTp with D40G, and 3.99 mM pdTp with D21E. These samples were further titrated with $CoCl_2$, measuring the increases in the $1/T_1$ and $1/T_2$ values of the 3′- and 5′-phosphates of pdTp. The data for both nucleotides were analyzed by plotting the increases in the relaxation rates against the increases in concentration of Co^{2+} bound in the respective ternary complexes. The slopes obtained this way, when multiplied by the total nucleotide concentration, yielded the normalized relaxation rates $1/fT_{1P}$ and $1/fT_{2P}$, in which the factor f is defined as [bound metal ion]/[total nucleotide]. The normalized relaxation rates of the ternary complexes were then corrected by subtracting the small paramagnetic effects in binary Co^{2+}–nucleotide complexes to yield $(1/fT_{1P})_{corr}$ and $(1/fT_{2P})_{corr}$. These small corrections, at most 10%, were based on the known distribution of Co^{2+} among its binary and ternary complexes, as calculated from the respective dissociation constants (Table III) together with measured paramagnetic effects of Co^{2+} on $1/T_1$ and $1/T_2$ of the phosphorus in the binary Co^{2+}–TMP and Co^{2+}–pdTp complexes.

^{31}P NMR spectra were obtained at 101.25 MHz by using 12-bit analog to digital conversion, collecting 8K or 16K data points over a spectral width of 2000 or 5000 Hz, with acquisition times of 2.0 or 1.6 s, respectively. Routine spectra were acquired by collecting 16–128 transients and using a 25-s delay to obtain fully relaxed spectra. The longitudinal relaxation rates ($1/T_1$) of ^{31}P resonances were measured by the nonselective saturation recovery method, which permitted shorter recycle times. Transverse relaxation rates ($1/T_2$) were derived from the widths of resonances at half-height ($\Delta\nu_{1/2}$), where $1/T_2 = \pi\Delta\nu_{1/2}$.

RESULTS

Effect of Ethylene Glycol on the Activities of Staphylococcal Nuclease and Its Mutants. To avoid solute aggregation upon freezing, samples of model compounds used in our low-temperature ESEEM studies contained ethylene glycol (50% v/v). With enzyme samples, it was found that ethylene glycol lengthened the damping time of the ESEEM, allowing improved spectral resolution. However, it also altered catalytic activity with Ca^{2+}. Table I shows the effects of ethylene glycol on the enzymatic activities of wild-type and mutant forms of staphylococcal nuclease at saturating levels of substrate and Ca^{2+}. At 24 °C, the V_{max} values for all the enzymes are reduced by ethylene glycol, except for the D40G mutant where it is increased. At 3 °C, significantly less reduction of activity for both the wild-type enzyme and the D40E mutant is observed. In contrast, all the others are activated. In the presence of ethylene glycol, there is a reduction of 2–4-fold in sensitivity to temperature, indicating lower activation energies for V_{max} (Table I). Since the effects of ethylene glycol on the V_{max} values for all the enzymes studied are relatively small, within 1 order of magnitude, its use to improve the resolution of the ESEEM experiments appears to be justified.

Electron Spin Echo Envelope Modulation (ESEEM) Studies of Model Compounds in ^2H_2O. When an appropriate sequence of microwave pulses is applied to a paramagnetic sample, such as a Mn^{2+}–ligand complex, a spin echo is observed, resulting from the refocusing of the electron spin magnetic vectors. When the pulse sequence is incremented in time, one obtains a time-dependent sequence of spin echoes, the amplitudes of which generate an envelope. If a nuclear spin is coupled to the electron spin, the envelope of the spin echoes does not decay monotonically but is modulated in a periodic manner related to the precession of the nuclear spin. This modulation varies in frequency, amplitude, and duration with different nuclear species, depending on their gyromagnetic ratio, their number, their distances from, and the nature of their coupling to the electron spin (Mims & Peisach, 1979, 1981). In addition, the depth of modulation is related to the

Table I: Effect of Ethylene Glycol and Temperature on the Maximal Velocity of Wild-Type and Mutant Staphylococcal Nuclease

mutant	50% ethylene glycol	act.[a] at 24 °C	fractional act. with ethylene glycol	act. at 3 °C	fraction act. with ethylene glycol	act. at 24 °C/ act. at 3 °C	E_a (kcal/mol)
wild type	−	0.763		0.0928		8.22	16
wild type	+	0.110	0.14	0.0342	0.37	3.22	9
D40G	−	0.0390		0.0044		8.86	17
D40G	+	0.0640	1.62	0.0256	5.82	2.50	7
D40E	−	0.0690		0.0193		3.58	10
D40E	+	0.0240	0.35	0.0160	0.83	1.50	3
T41P	−	0.0110		0.00113		9.73	18
T41P	+	0.0079	0.72	0.00283	2.51	2.79	8
D21E	−	0.000545		0.000214[b]		2.55[b]	11
D21E	+	0.000337	0.62	0.000270[b]	1.26	1.25[b]	3

[a] Activities are expressed as ΔAbs/(min·μg of enzyme) at saturating levels of the substrate DNA and Ca^{2+}. Saturation was checked by 2-fold variation of Ca^{2+} and DNA concentrations. [b] Due to the very low affinity of this mutant, these measurements were made at 10 °C. Hence, the ratios are activity at 24 °C/activity at 10 °C.

magnitude of nuclear spin such that the modulation depth for a deuteron is $^8/_3$ that for a proton, while the Larmor frequency is 6.5-fold lower (Mims et al., 1977). An echo envelope containing a number of modulation cycles can be Fourier transformed by established procedures (Mims, 1984) to give an ESEEM spectrum containing lines arising from electron–nuclear coupling in the sample.

In order to sort out the contributions of individual nuclei near a paramagnetic center, advantage is taken of the fact that the ESE envelope is a product function representing the magnetic interactions of all nuclei whose effects are related to number and distance from the paramagnet. By altering the chemical or isotopic composition in a single component of a sample, one can ratio ESEEM data against those for the original sample and in this way obtain modulation data for the difference (Zweier et al., 1979; Mims et al., 1984; McCracken et al., 1987).

Such an approach was taken in order to develop a method for examining water coordination to Mn^{2+} in binary and ternary metal–enzyme complexes. ESEEM studies were carried out on a pair of Mn^{2+} model compounds that differ from each other by a single water of coordination; Mn^{2+}–EDTA has a single coordinated water while Mn^{2+}–DTPA has none (Stezowski & Hoard, 1984). The ESE absorption envelope for each of these complexes is a product function containing contributions from ^{14}N and ^1H on the ligand and ^1H from coordinated and ambient water. When these complexes are prepared in ^2H_2O, the ^{14}N and nonexchangeable ^1H magnetic contributions from the ligand are identical, while the proton contributions from water and other exchangeable protons are replaced by those from deuterons. The ratio of data for a sample in ^2H_2O as compared to that in H_2O ideally contains spectroscopic contributions solely from exchangeable deuterium. ^{14}N and nonexchangeable proton contributions are removed by division (McCracken et al., 1987).[2]

The ratioed modulation data (Figure 2A) and the respective Fourier transforms (Figure 2B) for Mn^{2+}–EDTA in ^2H_2O and in H_2O contain a greater deuterium modulation than the ratioed data for Mn^{2+}–DTPA in ^2H_2O and in H_2O, as the metal ion in the former complex has a single coordinated water that is absent from the latter. The spectral difference, again obtained by a ratioing procedure, is the deuterium modulation for a single water in the primary coordination sphere of Mn^{2+} (Figure 2C,D). The assumption is made in this analysis that the modulation from ambient water for Mn^{2+} complexes of EDTA and DTPA is comparable.

[2] A negative peak in the ratioed ESEEM spectrum will be seen at the Larmor frequency for protons and is indicative of loss of protons in the sample in ^2H_2O.

There are two features of the deuterium ESEEM difference spectrum for inner coordination sphere ^2H_2O (Figure 2) that are worth noting. The first is that a comparison of the time domain data for this ^2H_2O (Figure 2C) with the corresponding data for Mn–EDTA, which contain spectral contributions from both coordinated and ambient ^2H_2O (Figure 2A, solid line), shows that the coordinated ^2H_2O contribution to the ESEEM accounts for only ~25% of the modulation depth (or amplitude) at the deuterium Larmor frequency. The second feature is the rapid damping of the deuterium ESEEM arising from inner-sphere deuterons, as seen in the time domain data (Figure 2C) and reflected in the broad line width of the corresponding Fourier transform (Figure 2D). For inner-sphere deuterons, the modulation decays more rapidly (Figure 2C) than for outer-sphere deuterons (Figure 2A, dashed line). Because the damping of the deuterium ESEEM is expected to become more rapid at shorter distances (Mims et al., 1984; McCracken et al., 1987), it is this characteristic of the data that is diagnostic of inner-sphere contributions.

The internal consistency of the method for quantitating the number of water ligands coordinated to Mn^{2+} was tested in the following way: If we consider hydrated Mn^{2+} as the hexaaquo coordinated ion, $Mn(H_2O)_6^{2+}$, then the deuterium modulation data for Mn^{2+} in ^2H_2O arises from two populations, from the six waters of hydration and from ambient water in outer coordination spheres. Using the ESEEM for the ambient water population from the ratioed deuterium modulation obtained for Mn^{2+}–DTPA (Figure 2A, dashed line), one can remove the ambient ^2H_2O contribution from the ESEEM of $Mn(^2H_2O)_6^{2+}$ to obtain the ESEEM data arising from the six coordinated ^2H_2O ligands. These results can then be compared directly to an ESEEM pattern obtained by raising the ESEEM contribution due to a single ^2H_2O ligand (Figure 2C) to the sixth power. Such agreement is shown in Figure 3, where parts A and B are the time domain data and corresponding Fourier transform obtained by raising the normalized ESEEM pattern of Figure 2C to the sixth power. For comparison, parts C and D of Figure 3 represent the inner-sphere deuterium modulation obtained from $Mn(^2H_2O)_6^{2+}$ after correction for ambient ^2H_2O contributions.

ESEEM Studies of Mn^{2+} Complexes of Staphylococcal Nuclease in ^2H_2O. Similar studies were carried out on Mn^{2+}–protein complexes. Ratios of modulation data for identical samples in ^2H_2O and in H_2O remove contributions from ^{14}N, ^{31}P, and nonexchangeable protons and give rise to modulations attributable to exchangeable protons in the vicinity of the paramagnetic center. For binary and ternary complexes of staphylococcal nuclease, a comparison of ratioed data for protein complexes in ^2H_2O and H_2O shows that the ternary complex of enzyme with Mn^{2+} and 3′,5′-pdTp has a

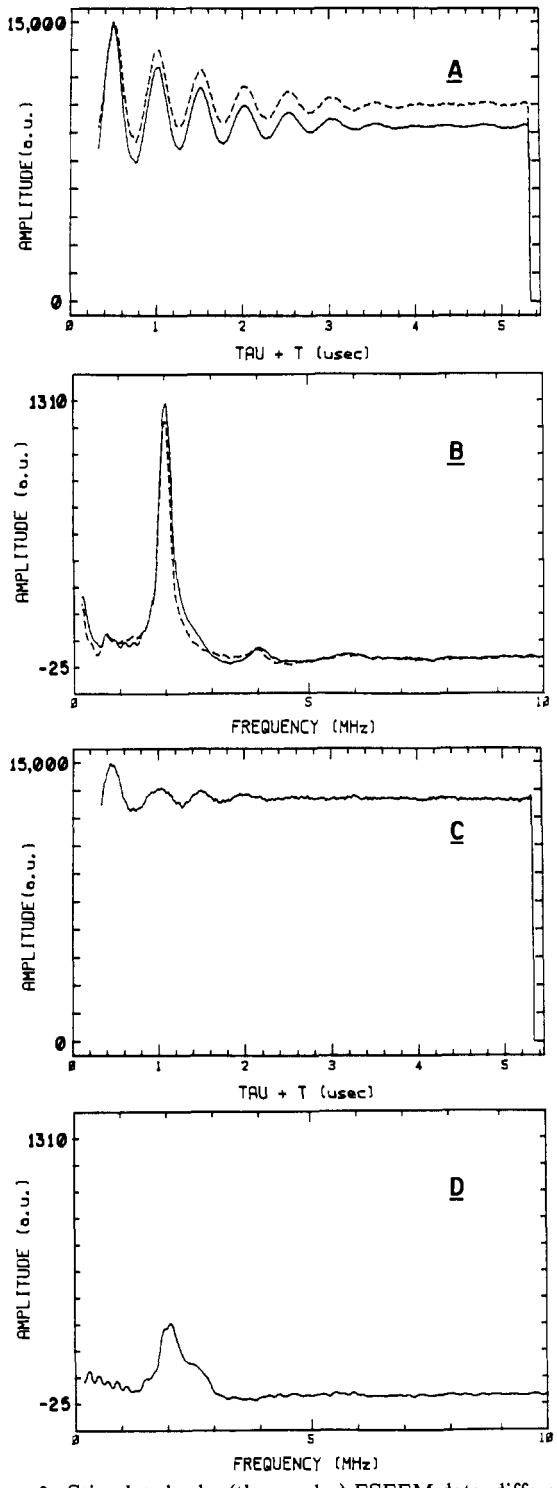

FIGURE 2: Stimulated echo (three pulse) ESEEM data, differences, and associated Fourier transforms for Mn^{2+}–EDTA and Mn^{2+}–DTPA in ^2H_2O. (A) Stimulated echo ESEEM data for Mn^{2+}–EDTA (solid line) and Mn^{2+}–DTPA (dashed line). For both samples the time domain data were corrected for background decay and modulations other than deuterium by ratioing data obtained for the sample in ^2H_2O with the data obtained for the sample in H_2O. (B) Fourier transform of the data in (A) for Mn^{2+}–EDTA (solid line) and for Mn^{2+}–DTPA (dashed line). (C) Difference between the two data sets shown in (A), obtained by dividing the Mn^{2+}–EDTA data set by the Mn^{2+}–DTPA data set. (D) Fourier transform of the difference in (C) attributed to a single ^2H_2O ligand plotted on the same scale indicated by arbitrary units as those transforms shown in (B). Components present were 1.0 mM $MnCl_2$, 1.2 mM NaEDTA or NaDTPA, and 40 mM Tris-HCl, pH 7.4, in 50% (v/v) ^2H_2O/ethylene glycol. Data were collected under the following conditions: microwave frequency, 8.75 GHz; magnetic field strength, 3000 G; microwave pulse power, 30 W; pulse width, 20 ns (full width at half-maximum); τ = 235 ns; sample temperature, 1.8K; each data point represents the average of 50 events.

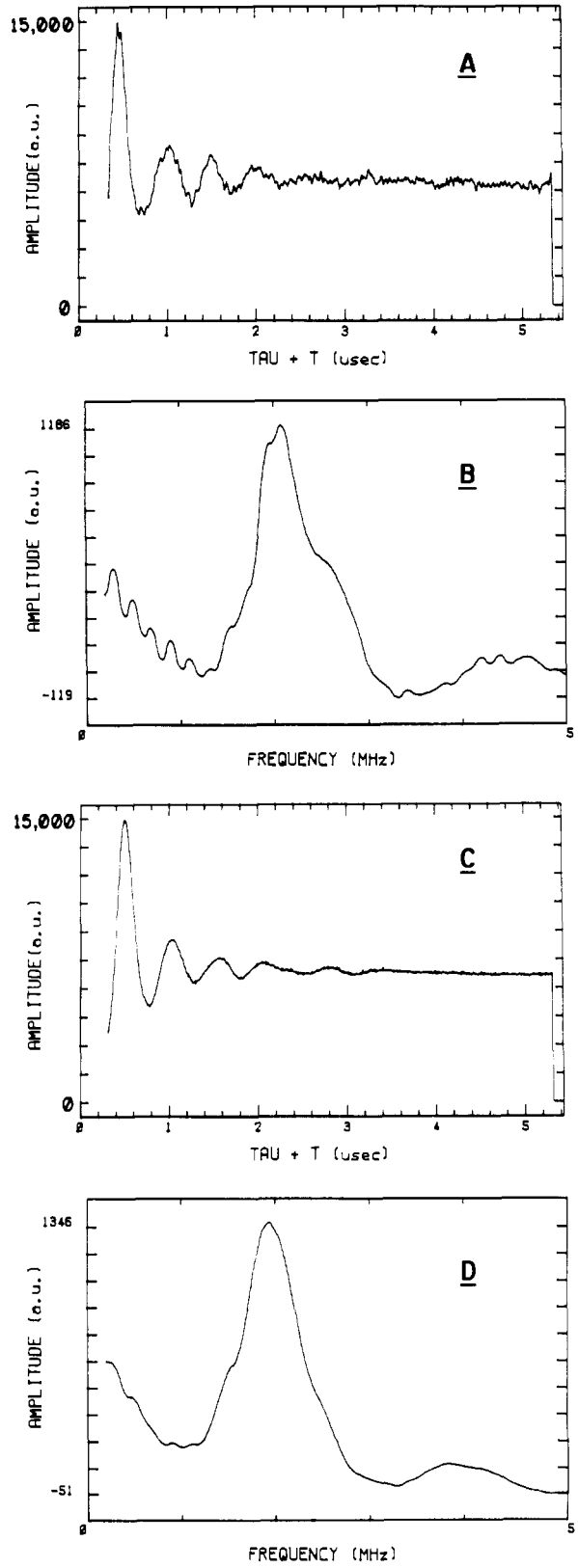

FIGURE 3: Comparison of the ESEEM data attributed to a single ^2H_2O ligand of Mn^{2+} with the data obtained with $Mn^{2+}(^2H_2O)_6$. (A) Stimulated echo ESEEM data obtained by raising the pattern shown in Figure 2C to the sixth power to obtain the equivalent of six ^2H_2O ligands. (B) Fourier transform of (A). (C) Stimulated echo ESEEM for $Mn^{2+}(^2H_2O)_6$ in 40 mM Tris-HCl and 50% (v/v) ^2H_2O/ethylene glycol. The data were corrected for both background decay and ESEEM due to outer-sphere deuterium by ratioing results for the ^2H_2O/ethylene glycol sample with data obtained for $Mn^{2+}(H_2O)_6$ in H_2O/ethylene glycol, and the ESEEM due to deuterium in the Mn^{2+}–DTPA sample (Figure 2A, dashed line). (D) Fourier transform of (C). Experimental conditions were identical with those in Figure 2.

Table II: Comparison of Number of Inner-Sphere Water Ligands (q) on Mn^{2+} in Binary and Ternary Complexes of Staphylococcal Nuclease As Found by Water Proton Relaxation and Pulsed EPR

	method		
	$1/T_{1P}$ (H_2O)[a]		ESEEM
complex	q (±0.1)	Δq^b (±0.2)	Δq^b (±0.2)
wild type–Mn^{2+}	0.8		
wild type–Mn^{2+}–pdTp	1.8	1.0	0.95
D40E–Mn^{2+}–pdTp	1.4	0.6	0.75
D40G–Mn^{2+}–pdTp	1.6	0.8	0.93
D21E–Mn^{2+}–pdTp	1.0	≤0.2	0.03
D21Y–Mn^{2+}–pdTp	2.2	1.4	0.96

[a] From Serpersu et al. (1987). [b] Δq indicates difference from binary Mn^{2+} complex of wild-type enzyme. The nonintegral values result from errors in the primary measurements of $1/T_{1P}$ and in the Fourier-transformed ESEEM spectra, as well as in the concentrations of the complexes, calculated from measured dissociation constants (Serpersu et al., 1987).

more intense deuterium modulation in the ratioed data than does the binary complex. The ratio of deuterium modulation data for ternary and binary complexes gives rise to a line centered at the deuterium Larmor frequency, the intensity and line width of which are consistent with those of a single water coordinated to Mn^{2+} (Figure 4A). Thus, the ternary complex has an added water of hydration over that in the binary complex, provided that contributions from ambient water are identical for both complexes. This result agrees well with earlier findings of ~1 fast exchanging water ligand on Mn^{2+} in the binary complex and ~2 in the ternary complex, based on the frequency dependence of $1/T_{1P}$ of water protons (Table II; Serpersu et al., 1987).

While the $1/T_{1P}$ method measures only the number of fast exchanging inner-sphere water ligands, the ESEEM method is useful for measuring the differences in the total number of inner-sphere water ligands, assuming that water protons are the major exchangeable species close to Mn^{2+} and that there is no difference in ambient water contributions between samples. The consistency of results obtained by both methods (Table II) suggests that all of the water ligands of the metal bound to staphylococcal nuclease exchange rapidly with the bulk solvent, a result consistent with the accessibility of the active site as found in the X-ray structure of the ternary enzyme–Ca^{2+}–pdTp complex (Cotton et al., 1979).

The high-resolution X-ray structure also reveals coordination of the metal by Asp 40, Asp 21, the amide carbonyl group of Thr 41, and the 5′-phosphate of pdTp (Figure 1). Similar coordination of Mn^{2+} is suggested by competition with Ca^{2+} and by the weaker binding of Mn^{2+} to the ligating mutants (Serpersu et al., 1986, 1987), although crystal and solution structures need not be identical. The two water ligands detected by NMR and inferred from ESEEM would complete the octahedral Mn^{2+} complex. The presence of only one water ligand in the binary enzyme–Mn^{2+} complex would require two additional ligands from the protein, possibly from Glu 43 and Asp 19 which are found to be only 4.6 and 4.9 Å, respectively, from the bound metal in the X-ray structure of the ternary complex (Figure 1), although the coordination of Asp 19 would require movement of the backbone.[3] Both the Glu 43 and Asp 19 ligands appear to be replaced by water upon binding of pdTp to the enzyme.

ESEEM analysis (Figure 4B) indicates the same number of water ligands coordinated to Mn^{2+} in ternary pdTp complexes of the wild-type enzyme as in the D40G, D40E (Figure 4B), and the D21Y mutants (Figure 4C). However, a comparison of ratioed deuterium data for the ternary complex of the D21E mutant enzyme with that for the ternary complex with the wild-type enzyme shows a difference consistent with one less ^2H_2O ligand on Mn^{2+} bound to the D21E mutant (Figure 4C). These data are also consistent with measurements based on the frequency dependence of $1/T_{1P}$ of water protons (Table II; Serpersu et al., 1987).

[3] P. Loll and E. Lattman, personal communication, 1988.

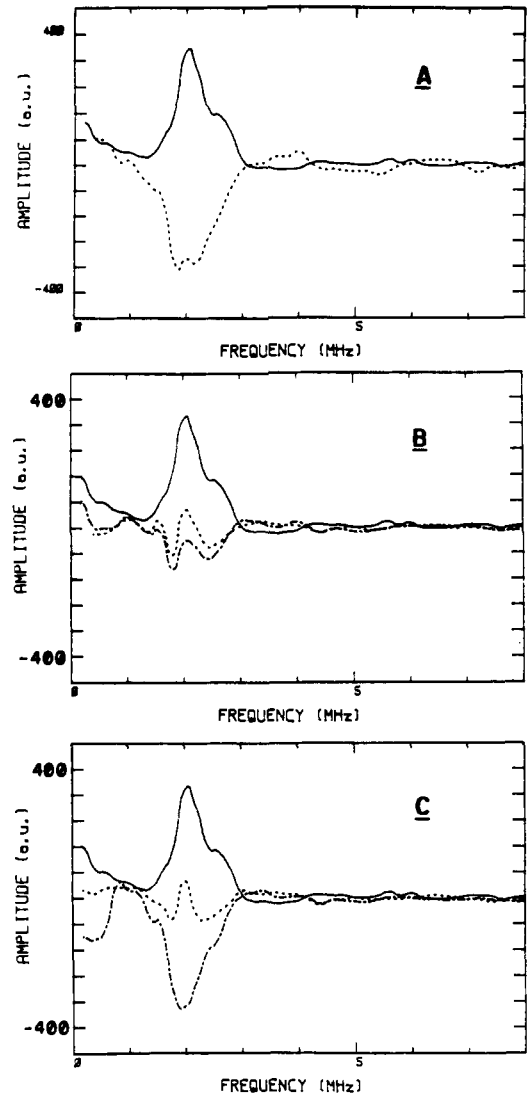

FIGURE 4: Differences in the number of ^2H_2O ligands of Mn^{2+} in complexes of staphylococcal nuclease from that of the ternary wild-type–Mn^{2+}–3′,5′-pdTp complex. The spectra are presented together with the ESEEM spectrum attributed to a single ^2H_2O molecule [solid lines in (A), (B), and (C)]. (A) Dashed line represents the difference spectrum between the binary wild-type–Mn^{2+} complex and the ternary wild-type–Mn^{2+}–pdTp complex. Difference spectra of ternary enzyme–Mn^{2+}–pdTp complexes of mutant enzymes from that of the ternary wild-type complex are shown in (B) for D40E (–·–) and D40G (···) and in (C) for D21E (–·–) and D21Y (···). Negative peaks in (A) and (C) indicate one less ^2H_2O ligand in these complexes compared to the ternary Mn^{2+} complex of the wild-type enzyme. The ternary complex samples were adjusted in concentration to contain 1.0 mM enzyme–Mn^{2+}–pdTp and 0.04 mM free Mn^{2+} by using 1.04 mM $MnCl_2$ and equimolar and appropriate concentrations of enzyme and pdTp, depending on the dissociation constant K_A', as follows: wild type, 1.3 mM; D40E, 1.2 mM; D40G, 1.7 mM; D21E, 1.6 mM; D21Y, 2.1 mM. The binary wild-type–Mn^{2+} sample contained 0.29 mM enzyme-bound Mn^{2+} and 0.04 mM free Mn^{2+}, on the basis of the K_D, resulting from 3.22 mM enzyme and 0.33 mM $MnCl_2$. Other components present and experimental conditions were as described in Figure 1. The corrected difference spectra were obtained as described in Figures 1 and 2. In all Fourier transformations, the depths of the modulations are scaled to the amplitude of the free induction decay, thus correcting for differences in Mn^{2+} concentration.

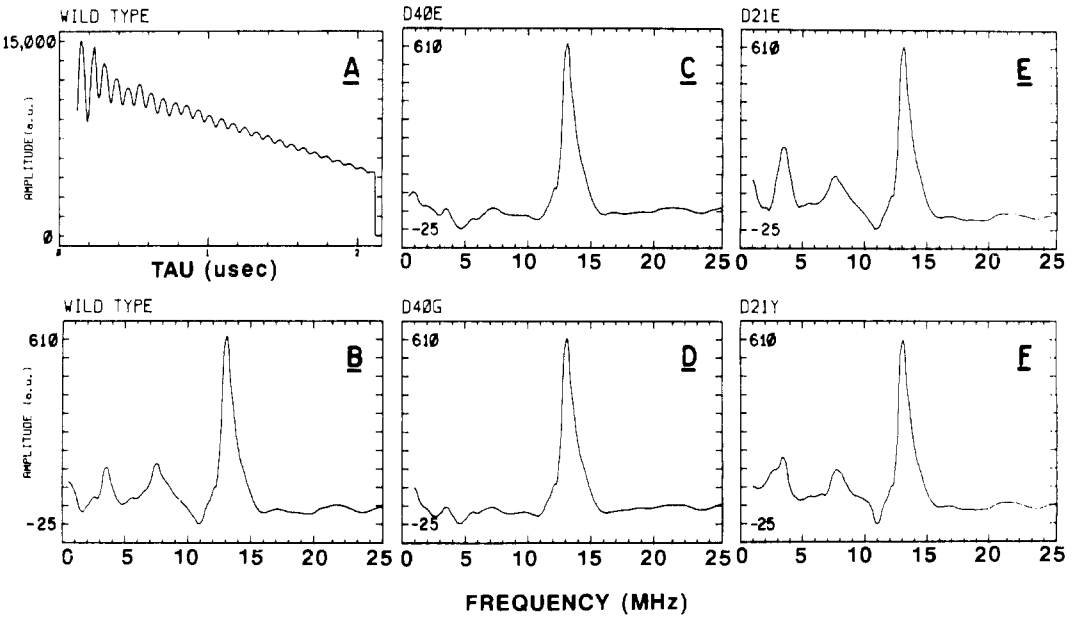

FIGURE 5: Two-pulse ESEEM data and Fourier transforms for ternary enzyme–Mn^{2+}–pdTp complexes in H_2O. (A) ESEEM data and (B) associated Fourier transforms for the ternary wild type–Mn^{2+}–pdTp complex. Fourier transforms of two pulse ESEEM data for ternary enzyme–Mn^{2+}–pdTp complexes of D40E (C), D40G (D), D21E (E), and D21Y (F). The components in each sample were as described in Figure 4, except that H_2O rather than ^2H_2O was present. Experimental conditions were identical with those given in Figure 2. The singlet at 12.8 MHz is assigned to protons, and the doublet in (B), (E), and (F) centered at 5.3 MHz with a splitting of 3.9 ± 0.3 MHz is assigned to ^{31}P of a phosphate ligand of enzyme-bound Mn^{2+}.

Our data suggest that in order to maintain the octahedral coordination geometry of Mn^{2+}, with no additional water ligands, there is substitution of the Asp 40 by Glu 40 in the ternary D40E complex and of Asp 21 by Tyr 21 in the ternary D21Y complex. An additional protein ligand is required to complete the metal coordination in the ternary enzyme–Mn^{2+}–pdTp complexes of the D40G and D21E mutants; the former lacks a potential metal ligand in a side chain, and the latter may have one less water ligand than found for the ternary complex of the wild-type enzyme (Figure 4C, Table II). Although structural data are not available, one might surmise the ligands on the basis of the catalytic activity of the mutant enzymes. It is suggested that Asp 19 rather than Glu 43 binds to Mn^{2+} in the D40G mutant, permitting Glu 43 to function as a general base. Mutations at position 43 have been shown to result in 3000-fold decreases in k_{cat}, whereas the D40G mutant has lost only a factor of 20–30 in k_{cat} (Hibler et al., 1987; Mildvan et al., 1988; Serpersu et al., 1986). In the case of D21E, which has lost a factor of 1500 in k_{cat}, a choice between Asp 19 and Glu 43 cannot be made on the basis of kinetic studies. Alternatively, unlike the ligands found in the crystalline enzyme (Figure 1), Asp 19 rather than Asp 21 might coordinate the metal in solution, and the longer Glu 21 could become an additional metal ligand in the D21E mutant. The D21Y mutant, which has lost a larger factor of about 2.9 × 10^4 in k_{cat}, is shown to retain two inner-sphere water ligands and therefore does not require additional ligands from the enzyme beyond the three found by X-ray analysis of the wild-type enzyme (Figure 1).

ESEEM Studies of Mn^{2+} Complexes of Staphylococcal Nuclease in H_2O. The electron spin echo envelope of an H_2O solution of the ternary enzyme–Mn^{2+}–dpTp complex of the wild-type enzyme shows both a high-frequency modulation and a low-frequency modulation (Figure 5A). Fourier transformation (Figure 5B) reveals a proton resonance at high frequency, 12.8 ± 0.1 MHz, arising from both inner-sphere and outer-sphere water molecules, as well as from protons of the protein. In addition, the lower frequency gives rise to a doublet centered at 5.3 ± 0.1 MHz, the Larmor frequency of ^{31}P, with a Fermi contact splitting of 3.9 ± 0.3 MHz corresponding to 1.4 ± 0.1 G. Comparable ^{31}P doublets are found in the Fourier-transformed electron spin echo modulation spectra of the ternary complexes of the D21E and D21Y mutants (Figure 5E,F). Such Fermi contact splitting by the ^{31}P nucleus indicates Mn^{2+}–phosphate bonding in which the unpaired electrons of Mn^{2+} are partially delocalized into an s-type orbital of phosphorus (LoBrutto et al., 1986). A ^{31}P doublet is not resolved in spectra of ternary complexes of the D40G and D40E mutants, nor is a 5.3-MHz singlet observed (Figure 5C,D), indicating weakened metal–phosphate interaction in these complexes as compared to the ternary complexes of the wild-type enzyme.

Paramagnetic Effects of Co^{2+} on ^{31}P Relaxation Rates in Binary Co^{2+}–Nucleotide and Ternary Enzyme–Co^{2+}–Nucleotide Complexes. The ^{31}P NMR spectrum of 5′-TMP consists of a triplet (J = 4.7 Hz) with a chemical shift 4.76 ppm downfield from H_3PO_4. The spectrum of 3′,5′-pdTp consists of a doublet (J = 7.8 Hz) at 3.93 ppm assigned to the 3′P and a triplet (J = 3.4 Hz) at 4.18 ppm assigned to the 5′P. An attempt was made to study the metal–phosphate interactions in ternary Mn^{2+} complexes of staphylococcal nuclease by an independent method, paramagnetic effects of Mn^{2+} on the longitudinal ($1/T_{1P}$) and transverse ($1/T_{2P}$) ^{31}P relaxation rates of TMP and pdTp. In favorable cases, such measurements yield metal to phosphorus distances (Mildvan & Gupta, 1978; Mildvan et al., 1980). However, no enhanced paramagnetic effects on phosphorus from the ternary enzyme–Mn^{2+}–TMP or enzyme–Mn^{2+}–pdTp complexes were detected, indicating these ternary complexes to be in slow exchange with the free ligands, TMP or pdTp. Ternary Mn^{2+} complexes of TMP and pdTp are known to exist from previous binding studies based on $1/T_{1P}$ of water protons (Serpersu et al., 1986, 1987) and from the present pulsed EPR data. Because of the high effective magnetic moment of Mn^{2+}, the longitudinal relaxation rate of a ligand such as TMP or pdTp in the binary Mn^{2+}–ligand complex may greatly exceed the ligand dissociation rate ($1/\tau_M$) from the inner coordination sphere of the ternary enzyme–Mn^{2+}–ligand complex. Under

Table III: Dissociation Constants of Co^{2+} from Binary Co^{2+}–Nucleotide and Ternary Enzyme–Co^{2+}–Nucleotide Complexes[a]

complex	K_A' (μM)	K_I (μM)
wild type–Co^{2+}–5′-TMP	158 ± 26	
wild type–Co^{2+}–pdTp	47 ± 22	
D21E–Co^{2+}–5′-TMP	91 ± 19	
D21E–Co^{2+}–pdTp	48 ± 12	
D40G–Co^{2+}–5′-TMP	585 ± 46[b]	
D40G–Co^{2+}–pdTp	69 ± 11[b]	
Co^{2+}–5′-TMP		4170 ± 560[b]
Co^{2+}–pdTp		209 ± 30[b,c]

[a] Average of values determined by competition with Mn^{2+} as detected by EPR and by $1/T_{1P}$ of water protons at 24 °C. $K_A' = ([Co^{2+}]\cdot[E\text{-}Nuc])/[E\text{-}Co^{2+}\text{-}Nuc]$, and $K_I = ([Co^{2+}][Nuc])/[Co^{2+}\text{-}Nuc]$. [b] Determined by EPR only. [c] Number of binding sites for Co^{2+} assumed to be 1.6 ± 0.2 as previously found for the Mn^{2+}–pdTp complex (Serpersu et al., 1986).

these conditions, the ligand in the ternary complex is undetectable by the NMR method. Slow exchange of TMP out of its ternary complex is especially noteworthy since this ligand is bound to the Mn^{2+} complex of staphylococcal nuclease an order of magnitude more weakly than is pdTp (Serpersu et al., 1986).

Such slow exchange of inner-sphere enzyme–metal–ligand complexes is frequently observed with Mn^{2+} (Melamud & Mildvan, 1975). To observe the ligand in the ternary complex when this occurs, a paramagnetic metal with a much smaller effective magnetic moment, such as Co^{2+}, must be used, provided Co^{2+} occupies the same binding site as Mn^{2+} and Ca^{2+} in staphylococcal nuclease. Because of the markedly decreased paramagnetic effects of Co^{2+} on $1/T_1$ and $1/T_2$, the relaxation rates of the ligand in the binary Co^{2+}–ligand and ternary enzyme–Co^{2+}–ligand complexes are generally reduced to values lower than the escape rate of the ligand from the inner coordination sphere of the ternary complex, rendering the paramagnetic effects on the enzyme-bound ligand detectable by NMR methods.

As previously found for Mn^{2+} (Serpersu et al., 1986, 1987), Co^{2+} also fails to activate staphylococcal nuclease but is a linear competitive inhibitor with respect to Ca^{2+}. The K_i values of Co^{2+} with the wild-type enzyme and the D40G and D21E mutants are 0.35, 0.38, and 0.39 mM respectively (data not shown). Active-site binding of Co^{2+} is independently established by the competitive displacement of Mn^{2+} by Co^{2+} from the ternary enzyme–Mn^{2+}–TMP and enzyme–Mn^{2+}–pdTp complexes of the wild and mutant enzymes, as detected by increases in the intensity of the EPR spectrum of free Mn^{2+} and by decreases in $1/T_{1P}$ of water protons. Table III gives the dissociation constant of Co^{2+} from the ternary enzyme–Co^{2+}–nucleotide complexes (K_A') as well as the dissociation constants (K_I) of the binary Co^{2+}–TMP and Co^{2+}–pdTp complexes, also determined by competition with Mn^{2+}, as monitored by EPR.

Titrations with $CoCl_2$ measuring $1/T_1$ of the ^{31}P resonance of TMP in the absence or presence of staphylococcal nuclease (Figure 6A) indicate that the enzyme enhances the paramagnetic effects of Co^{2+} on $1/T_1$. A comparison of the slopes of the titration curves yields an observed enhancement factor (ϵ^*) of 2.8-fold. Smaller enhancement factors are found for the D21E mutant ($\epsilon^* = 2.2$) and the D40G mutant ($\epsilon^* = 1.6$). In all cases, the enhancements observed with Co^{2+} indicate the presence of ternary enzyme–Co^{2+}–TMP complexes.

The concentrations of the binary Co^{2+}–TMP and ternary enzyme–Co^{2+}–TMP complexes present in the system, calculated from the K_I and K_A' values (Table III), together with the paramagnetic effect of Co^{2+} on $1/T_1$ in the binary Co^{2+}–TMP complex (Figure 6A) were used to evaluate $(1/fT_{1P})_{corr}$, the corrected paramagnetic contribution to the longitudinal relaxation rate in the ternary TMP complexes of the wild-type and mutant enzymes (Table IV). A similar approach was used to evaluate $(1/fT_{2P})_{corr}$, the corrected paramagnetic contributions to the transverse relaxation rates in each ternary complex (Table IV). In all cases $(1/fT_{2P})_{corr}$, which sets a lower limit to $1/\tau_M$, the exchange rate of TMP out of the ternary complex, exceeds $(1/fT_{1P})_{corr}$ by more than an order of magnitude. Hence, $(1/fT_{1P})_{corr}$ is the relaxation rate of the bound ligand and may therefore be used to determine the Co^{2+}–phosphorus distances in the ternary complexes, provided the outer-sphere contribution to $(1/fT_{1P})_{corr}$ is small and the correlation time (τ_c) for electron–nuclear dipolar interaction can be evaluated. Displacement of TMP from the ternary enzyme–Co^{2+}–TMP complexes by the tighter binding ligand pdTp abolishes the paramagnetic effects of Co^{2+} on the ^{31}P relaxation rates of TMP, indicating negligible outer-sphere contributions to $(1/fT_{1P})_{corr}$ and $(1/fT_{2P})_{corr}$ in

Table IV: Corrected ^{31}P Relaxation Rates, Correlation Times, and Co^{2+} to Phosphorus Distances in Ternary Co^{2+} Complexes of Staphylococcal Nuclease

complex	$(1/fT_{1P})_{corr}$ (s^{-1})		$10^4(1/fT_{2P})_{corr}$ (s^{-1})		$10^{-23}B^a$ (s^{-2})	$10^{13}\tau_v{}^a$ (s)	$10^{12}\tau_c{}^{a,b}$ (s)	$10^{12}f(\tau_c)^c$ (s)	r^d (Å)	
	5′P	3′P	5′P	3′P					5′P	3′P
wild type–Co^{2+}–5′-TMP	382 ± 41		0.77 ± 0.22		10.5	5.96	0.69 ± 0.08	6.53 ± 0.76	3.3 ± 0.7	
D40G–Co^{2+}–5′-TMP	124 ± 14		6.31 ± 0.47		1.33	6.68	5.1 ± 2.1	21.8 ± 8.9	4.9 ± 1.0	
D21E–Co^{2+}–5′-TMP	404 ± 44		1.52 ± 0.22		11.9	5.01	0.65 ± 0.02	6.19 ± 0.20	3.3 ± 0.7	
wild type–Co^{2+}–pdTp	1443 ± 132	81.5 ± 8	2.15 ± 0.46	1.29 ± 0.64	9.42	5.96	0.77 ± 0.11	7.19 ± 0.93	2.7 ± 0.5	4.4 ± 0.9
D40G–Co^{2+}–pdTp	793 ± 108	147 ± 15	11.8 ± 1.5	5.1 ± 2.4	1.77	4.21	4.53 ± 0.59	20.5 ± 2.5	3.6 ± 0.7	4.7 ± 0.9
D21E–Co^{2+}–pdTp	2036 ± 164	189 ± 19	1.36 ± 0.06	1.14 ± 0.40	10.5	5.31	0.76 ± 0.02	7.11 ± 0.20	2.6 ± 0.5	3.8 ± 0.8

[a] Determined by the frequency dependence of the normalized longitudinal relaxation rates ($1/fT_{1P}$) of water protons at 15, 24.3, 42, 59.8, 250, and 360 MHz and analyzed according to the following equations (Mildvan & Gupta, 1978; Mildvan et al., 1980): $1/fT_{1P} = q(C/r)^6 f(\tau_c)$, $f(\tau_c) = 3\tau_c/(1 + \omega_I{}^2\tau_c{}^2) + 7\tau_c/(1 + \omega_s{}^2\tau_c{}^2)$, and $1/\tau_c = 1/\tau_s = B[\tau_v/(1 + \omega_s{}^2\tau_v{}^2) + 4\tau_v/(1 + 4\omega_s{}^2\tau_v{}^2)]$, where q is the ligand/metal stoichiometry in the complex, C is a product of physical constants equal to 895 ± 125 for Co^{2+} proton interactions and 662 ± 93 for Co^{2+}–^{31}P interaction, r is the metal–nucleus distance, τ_c is the dipolar correlation time, ω_I and ω_s are the nuclear and electron precession frequencies, τ_s is the longitudinal electron spin relaxation time, B is the zero field splitting parameter, and τ_v is a time constant for ligand motion that modulates B. The C values are based on the assumption that the g value for high-spin Co^{2+} lies within the range 4 ± 2. [b] τ_c at 5.87 T, i.e., at 250 MHz for protons and at 101.3 MHz for ^{31}P. [c] $f(\tau_c)$ calculated for ^{31}P at 101.3 MHz. [d] Errors shown are in the absolute distances, which include a 14% contribution due to the anisotropic g values of Co^{2+} and a 4%–7% contribution due to experimental errors in the measurements of $1/fT_{1P}$, τ_c, and K_A'. Errors in distances are smaller than errors in the measured parameters, due to the sixth root relationship in the Solomon–Bloembergen equation. If the orientation of the g tensor of Co^{2+} were the same in all of the complexes, the errors in the relative distances would be ±4%–7%.

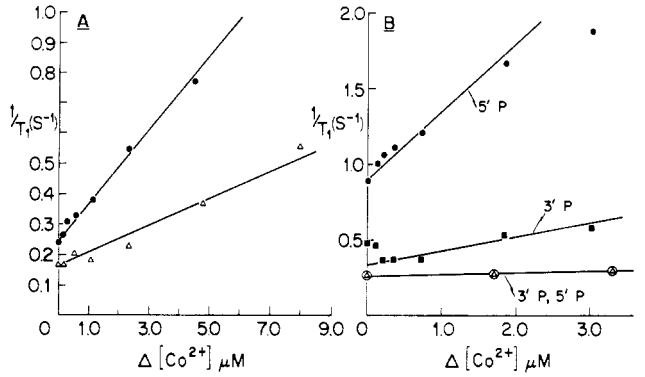

FIGURE 6: Paramagnetic effects of Co^{2+} on the phosphorus resonances of TMP (A) and pdTp (B) in the absence and presence of wild-type staphylococcal nuclease. Components present in (A) were 4.15 mM TMP (△) and 4.15 mM TMP and 0.2 mM wild-type staphylococcal nuclease (●) and in (B) 3.63 mM 3′,5′-pdTp (3′P △, 5′P ○) 3.63 mM 3′,5′-pdTp, 0.2 mM wild-type staphylococcal nuclease (3′P ■, 5′P ●). Other components present were 4.15 mM TMP, 28 mM NaCl, 10 mM Na^+ TES, pH 7.4, and 20% ^2H_2O. ^{31}P spectra were obtained at 101.25 MHz by using 16–28 transients with 16K data points, spectral width of 5000 Hz, an acquisition time of 1.6 s, and 12-bit A/D conversion. T = 24 °C.

all cases. In complexes of high-spin Co^{2+}, the correlation time τ_c for electron–nuclear dipolar interaction is dominated by the short electron spin relaxation time (τ_S) of Co^{2+}. Hence τ_c may be evaluated by the frequency dependence of $1/T_{1P}$ of water protons in the same complex. Such studies were made with ternary enzyme–Co^{2+}–TMP complexes of the wild type and all of the mutant enzymes permitting calculation of the Co^{2+}–P distances (Table IV).

Titrations of staphylococcal nuclease–pdTp complexes with Co^{2+}, measuring the paramagnetic effects on $1/T_1$ and $1/T_2$ of the 3′- and 5′-phosphorus resonances (Figure 6B) revealed very large enhancements by the wild-type and mutant enzymes of the paramagnetic effects of Co^{2+} on the phosphorus relaxation rates of pdTp. The enhancement factors for the 5′P of pdTp of 37.9, 49.1, and 21.2 with the wild-type enzyme and the D21E and the D40G mutants, respectively, greatly exceed those found with TMP, reflecting both a greater occupancy by Co^{2+} and stronger Co^{2+}–P interactions in the ternary pdTp complexes. The ϵ^* values for the 3′P in the ternary complexes of the wild-type enzyme and the D21E and D40G mutants are 8.8, 7.8, and 9.7 respectively, reflecting weaker Co^{2+}–P interactions with the 3′-phosphate. As with TMP, the concentrations of Co^{2+} in the binary Co^{2+}–pdTp complexes and in the ternary enzyme–Co^{2+}–pdTp complexes were calculated from the K_1 and K_A' values (Table III), permitting an evaluation of $(1/fT_{1P})_{corr}$ and $(1/fT_{2P})_{corr}$ for the 3′P and 5′P in each ternary complex (Table IV). In all cases $(1/fT_{2P})_{corr}$ greatly exceeded $(1/fT_{1P})_{corr}$, by more than an order of magnitude, establishing that $(1/fT_{1P})_{corr}$ is the relaxation rate of the bound ligand and is therefore suitable for distance calculations. Table IV gives the correlation times determined from the frequency dependence of $1/T_{1P}$ of water protons and the calculated Co^{2+} to P distances in the ternary pdTp complexes.

Comparison of Co^{2+} to P Distances in Staphylococcal Nuclease Complexes with Distances in Model Complexes. Significantly shorter distances from Co^{2+} to the 5′P of pdTp and TMP are found in the ternary Co^{2+} complexes of the wild-type enzyme and the D21E mutant than in the D40G mutant. These findings are in excellent agreement with the results of the ESEEM studies of the corresponding Mn^{2+} complexes, which revealed Mn^{2+} to P Fermi contact interaction in the wild-type enzyme and in the D21E mutant but not in

Table V: Co^{2+} to Phosphorus Distances from X-ray Structures and Model Building of Co^{2+}–Phosphate Complexes

complex	distance (Å)	av (Å)
inner-sphere monodentate		
$Co^{2+}(H_2PO_4)_2{\cdot}2H_3PO_4$	3.27[a]	
	3.34[a]	
$Co^{2+}(O_2PF_2)_2{\cdot}2MeCN$	3.35[b]	
Co^{2+}–5′-CMP(H_2O)	3.29[c]	3.31 ± 0.04
inner-sphere bidentate		
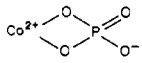	2.7 ± 0.1[d]	2.7 ± 0.1
second sphere, intervening H_2O		
$Co^{2+}(H_2O)_5$–5′-IMP·$2H_2O$	4.72[e]	
$Co^{2+}(H_2O)_5$–5′-dIMP·$2H_2O$	4.78[f]	4.75 ± 0.03

[a] Coordinates from Herak et al. (1983). Crystal showed two different Co–phosphate interactions with the distances shown. [b] Coordinates from Begley et al. (1985). [c] Coordinates from Clark and Orbell (1978). [d] From model building, assuming Co^{2+}–O bond distances of 2.1 Å, an O–P distance of 1.5–1.6 Å, and an O–P–O bond angle of 109°. The X-ray structure of an inner-sphere bidentate phosphate complex of Co^{3+}, namely, Co^{3+}(ethylenediamine)PO_4^{3-}, reveals a Co^{3+} to P distance of 2.55 Å (Anderson et al., 1977). [e] Coordinates from Aoki (1975). [f] Coordinates from Poojary and Manohar (1986).

the D40G mutant (Figure 5). High-resolution X-ray studies of small Co^{2+}–phosphate complexes and model-building studies, summarized in Table V, reveal Co^{2+} to P distances of 3.31 ± 0.04 Å for inner-sphere monodentate phosphate complexes, 2.7 ± 0.1 Å for an inner-sphere bidentate complex in which two oxygens of the phosphate ligand are simultaneously coordinated to Co^{2+}, and 4.75 ± 0.03 Å for second-sphere complexes with an intervening water ligand.

Co^{2+} to phosphorus distances in the ternary enzyme–Co^{2+}–TMP complexes suggest monodentate phosphate coordination to metal in the wild-type enzyme and in the D21E mutant and second-sphere coordination in the D40G mutant. Distances measured in the staphylococcal nuclease–Co^{2+}–pdTp complexes suggest bidentate metal coordination of the 5′-phosphate with the wild-type enzyme and with the D21E mutant and monodentate coordination of the 5′-phosphate to metal with the D40G mutant. For the corresponding Mn^{2+} complexes, in which distances could not be measured, such bidentate phosphate coordination and the resulting shorter metal–phosphorus distance would permit more favorable overlap of a half-filled d orbital of Mn^{2+} with the vacant 4s orbital of phosphorus, permitting the observed contact interaction.

The 3′-phosphate of pdTp appears to be predominantly in the second coordination sphere of Co^{2+} in the three pdTp complexes studied, as judged by comparing the measured distances (Table IV) with those found in model complexes (Table V). Even in the case of the D21E–Co^{2+}–pdTp complex, because of the $1/r^6$ dependence of $(1/fT_{1P})_{corr}$, the distance of 3.8 Å, which is shorter than that found in the wild-type enzyme, could result from the averaging of 64% second-sphere (4.75 Å) and 36% inner-sphere complexation (3.31 Å).

Discussion

Since ethylene glycol was used to improve the signal/noise ratio in the low-temperature pulsed EPR studies, a detailed examination of its effects on enzymatic activity was necessary (Table I). The lowering of V_{max} of staphylococcal nuclease and of most of its mutants at 24 °C in 50% (v/v) ethylene glycol and the diminution of this inhibitory effect at lower temperatures may be ascribed to a direct, nonpolar interaction of ethylene glycol with the protein tending to loosen or unfold hydrophobic internal groups (Collins & Washabaugh, 1985). The unusual activation of the D40G mutant at 24 °C and of

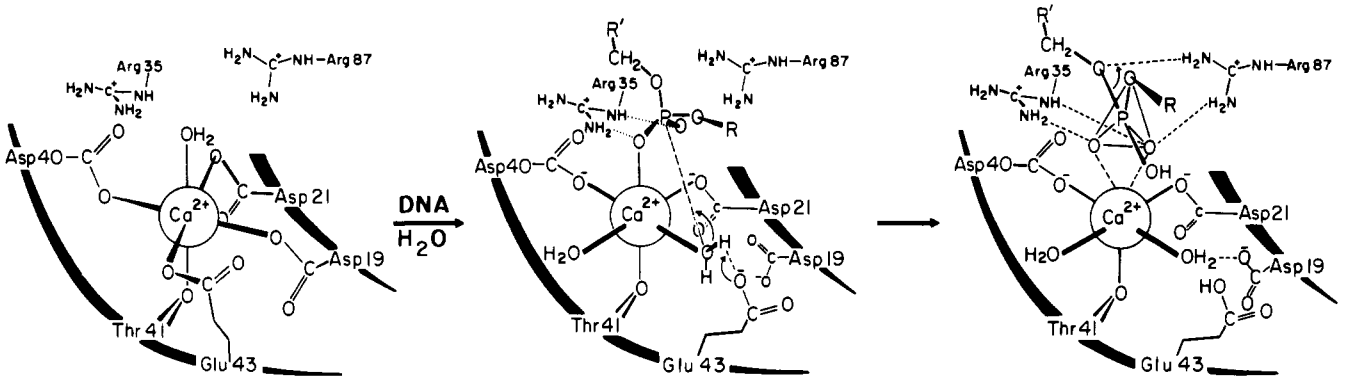

FIGURE 7: Mechanism of substrate binding and hydrolysis catalyzed by staphylococcal nuclease. The left panel shows the binary complex, and the center panel shows the ternary complex. The right panel shows the transition state that leads to the enzyme–product complex in which R–PO_3OH is coordinated to Ca^{2+}. When both products leave, Glu 43 and probably Asp 19 coordinate to the metal, replacing water ligands. This mechanism is based on the present structural studies of Mn^{2+} and Co^{2+} complexes and on kinetic studies of enzymes mutated at positions 21, 35, 40, 41, 87 (Serpersu et al., 1986, 1987) and 43 (Hibler & Gerlt, 1986; Hibler et al., 1987; Mildvan et al., 1988).

most of the mutant enzymes at 3 °C requires a second, opposing effect of ethylene glycol. Hence, additional activating effects of ethylene glycol must be postulated, such as an increase in microscopic viscosity or a decrease in the dielectric constant of the solvent at the active site. The former effect is possible, as indicated by a significant increase in the longitudinal relaxation rate of water protons from 0.39 to 0.90 s^{-1} in the presence of 50% ethylene glycol, in which the carbon-bound protons were deuteriated.[4] This observation indicates a corresponding increase in the rotational correlation time of water molecules. Increasing the microscopic viscosity and thereby decreasing mobility at the active site could, in principle, lower the entropy barrier to the rate-limiting nucleophilic attack by OH^- on phosphorus (Figure 7), restoring some of the activity lost in the mutant enzymes. Lowering the dielectric constant might accelerate the reaction by strengthening the electrophilic effects of the metal, of Arg 35 on the phosphodiester in the ground state, and of Arg 87 in the transition state. The effects of ethylene glycol on both the viscosity and the dielectric constant could also contribute to the inhibition of the wild-type enzyme, slowing the rate-limiting dissociation of the product. Because of the decreased inhibition or greater activation of all of the enzyme forms at low temperature (Table I), the use of ethylene glycol to improve the signal/noise ratio in the EPR data is reasonable and justified in the present case.

The ESEEM studies in ^2H_2O with the model compounds $Mn(^2H_2O)_6^{2+}$, (^2H_2O)MnEDTA, and MnDTPA establish the value of this pulsed EPR method for counting the total number of residual water ligands coordinated to Mn^{2+} in various complexes, provided that appropriate controls are available to correct for the large contributions from outer-sphere water and other exchangeable protons. Pulsed EPR in ^2H_2O thus provides a valuable supplement to pulsed NMR studies in H_2O of $1/T_{1P}$ of water protons, which detect only fast exchanging water ligands of Mn^{2+}, i.e., thost that dissociate from Mn^{2+} at rates exceeding $\sim 10^6$ s^{-1}. The agreement in the results obtained by the two methods with the Mn^{2+} complexes of staphylococcal nuclease and its mutants (Table II) suggests that all of the water ligands to Mn^{2+} in this system are in fast exchange. However, fast exchange of water ligands of Mn^{2+} is not always observed. In transition-state analogue complexes of creatine kinase, less than 0.5 water ligand of Mn^{2+} was determined from $1/T_{1P}$ measurements of water protons (Reed et al., 1972). In contrast, three water ligands were detected by EPR analysis of superhyperfine splitting by $H_2{}^{17}O$, indicating that the three water ligands on Mn^{2+} are in slow exchange on the time scale defined by $1/T_{1P}$ (Reed & Leyh, 1980).

Our finding of one less water ligand on Mn^{2+} in the binary Mn^{2+} complex than on the ternary complex of wild-type staphylococcal nuclease requires two additional ligands to Mn^{2+} from the enzyme, possibly Glu 43 and Asp 19, in order to maintain octahedral coordination geometry. Our recent finding that mutation of the Glu 43 residue to serine significantly weakens the binding of Mn^{2+} and Ca^{2+} to the enzyme supports this view (Mildvan et al., 1988). The coordination of the 5′-phosphate of the substrate analogue pdTp and, presumably, the phosphodiester phosphate of the DNA substrate releases both these ligands, permitting the coordination of an additional water ligand, possibly the attacking water molecule, and allows Glu 43 to function as a general base (Figure 7). For octahedral metal coordination, additional ligands to Mn^{2+} from the protein are also required in the ternary enzyme–Mn^{2+}–pdTp complexes of the D40G and D21E mutants. Since no X-ray structures of the corresponding binary and ternary Ca^{2+} complexes are available, it is not certain that Ca^{2+} behaves in the same way as does Mn^{2+}.

The strong Mn^{2+}–phosphate interactions demonstrated by Fermi contact splitting in the pulsed EPR studies of the ternary pdTp complexes (Figure 5) and independently detected by the short Co^{2+} to P distances measured by ^{31}P relaxation in the corresponding Co^{2+} complexes (Table IV) are most simply explained by bidentate coordination of the 5′P of pdTp by the metal (Table V). However, it should be noted that Mn^{2+}–phosphate contact splittings similar to those measured in this work by ESEEM methods may arise from monodentate coordination.[5] Alternative structures involving distorted geometries or unusually short metal–oxygen or O–P bonds, while not excluded, seem less likely. Although we could find no crystal structure of a bidentate Co^{2+}–phosphate complex in the literature, bidentate nitrate complexes of Co^{2+}, Mn^{2+}, Cu^{2+}, and Zn^{2+} have been well characterized (Wells, 1984), and a bidentate Co^{3+}–phosphate complex has been described (Anderson et al., 1977). Moreover, in the suggested pentacovalent phosphorane transition state, the trigonal geometry of the three equatorial oxygens around the phosphorus is very similar to that of nitrate. Hence, bidentate coordination may selectively stabilize the phosphorane transition state of staphylococcal nuclease and thereby contribute to the activating effect of the metal ion (Figure 7).

[4] E. H. Serpersu and A. S. Mildvan, unpublished observations, 1988.

[5] G. H. Reed, personal communication, 1988.

In a model study, a strained, bidentate *p*-nitrophenyl phosphate complex of Co^{3+} shows a 10^9-fold acceleration of base hydrolysis of this ester relative to that of the uncoordinated ester (Anderson et al., 1977). Regardless of the precise nature of the strong metal–phosphate interaction in staphylococcal nuclease, its presence contributes at most 1 order of magnitude to enzymatic activity, since the D40E and D40G mutants that lack this interaction have lost factors of only 12 and 30, respectively, in k_{cat}, compared to the wild-type enzyme. The D21E and D21Y mutants, which retain the strong metal–phosphate interaction, have lost much larger factors of 1500 and 29 000 in k_{cat}, which we have previously ascribed to occlusion by the enlarged ligand at position 21, of the binding site for the attacking water molecule (Serpersu et al., 1987) (Figure 7). The present data, which reveal intact metal–phosphate interactions on these mutant enzymes, support this view.

ACKNOWLEDGMENTS

We are grateful to David Shortle for providing us with strains of *E. coli* that overproduce wild-type and ligating mutants of staphylococcal nuclease and for valuable discussions, to Pat Loll and Eaton Lattman for comments on their refined X-ray structure of the ternary enzyme–Ca^{2+}–3′,5′-pdTp complex, and to Jeremy Berg for helpful advice.

REFERENCES

Anderson, B., Milburn, R. M., Harrowfield, J. Mac B., Robertson, G. M., & Sargeson, A. M. (1977) *J. Am. Chem. Soc. 99*, 2652–2661.

Aoki, K. (1975) *Bull. Chem. Soc. Jpn. 48*, 1260–1271.

Begley, M. J., Dave, M. F. A., Hibbert, R. C., Logan, N., Nunn, M., & Sowerby, D. B. (1985) *J. Chem. Soc., Dalton Trans. 1985*, 2433–2436.

Bradford, M. M. (1976) *Anal. Biochem. 72*, 248–254.

Clark, G. R., & Orbell, J. D. (1978) *Acta Crystallogr., Sect. B: Struct. Crystallogr. Cryst. Chem. B34*, 1815–1822.

Cotton, F. A., Hazen, E. E., & Legg, M. J. (1979) *Proc. Natl. Acad. Sci. U.S.A. 76*, 2551–2555.

Cuatrecasas, P., Fuchs, S., & Anfinsen, C. B. (1967) *J. Biol. Chem. 242*, 1541–1547.

Hall, J. L., Swisher, J. A., Brannon, D. G., & Linden, T. M. (1962) *Inorg. Chem. 1*, 409–413.

Hanlon, S., Chan, A., & Berman, S. (1978) *Biochim. Biophys. Acta 519*, 526–536.

Herak, R., Prelesnik, B., Curic, M., & Djurik, S. (1983) *Z. Kristallogr. 164*, 25–30.

Hibler, D. W., Stolowich, J. N., Reynolds, M. A., Gerlt, J. A., Wilde, J. A., & Bolton, P. H. (1987) *Biochemistry 26*, 6278–6286.

LoBrutto, R., Smithers, G. W., Reed, G. H., Orme-Johnson, W. H., Pan, S. L., & Leigh, J. S. (1986) *Biochemistry 25*, 5654–5660.

McCracken, J., Peisach, J., & Dooley, D. M. (1987) *J. Am. Chem. Soc. 109*, 4064–4072.

McCracken, J., Serpersu, E. H., Peisach, J., & Mildvan, A. S. (1988) *FASEB J. 2*, Abstract 1697, A588.

Melamud, E., & Mildvan, A. S. (1975) *J. Biol. Chem. 250*, 8193–8201.

Mildvan, A. S., & Gupta, R. K. (1978) *Methods Enzymol. 49G*, 322–359.

Mildvan, A. S., Granot, J., Smith, G. M., & Liebman, M. N. (1980) *Adv. Inorg. Biochem. 2*, 211–236.

Mildvan, A. S., Serpersu, E. H., Hibler, D. W., & Gerlt, J. A. (1988) *FASEB J. 2*, Abstract 1698, A588.

Mims, W. B. (1984) *J. Magn. Reson. 59*, 291–306.

Mims, W. B., & Peisach, J. (1976) *Biochemistry 15*, 3863–3869.

Mims, W. B., & Peisach, J. (1981) in *Biological Magnetic Resonance* (Berliner, L. J., & Reuben, J., Eds.) Vol. III, pp 213–263, Plenum, New York.

Mims, W. B., Peisach, J., & Davis, J. L. (1977) *J. Chem. Phys. 66*, 5536–5550.

Mims, W. B., Davis, J. L., & Peisach, J. (1984) *Biophys. J. 45*, 755–766.

Peisach, J., Mims, W. B., & Davis, J. L. (1979) *J. Biol. Chem. 254*, 12379–12389.

Poojary, M. D., & Manohar, H. (1986) *J. Chem. Soc., Dalton Trans. 1986*, 309–312.

Reed, G. H., & Leyh, T. S. (1980) *Biochemistry 19*, 5472–5480.

Reed, G. H., Diefenbach, H., & Cohn, M. (1972) *J. Biol. Chem. 247*, 3066–3072.

Serpersu, E. H., Shortle, D., & Mildvan, A. S. (1986) *Biochemistry 25*, 68–77.

Serpersu, E. H., Shortle, D., & Mildvan, A. S. (1987) *Biochemistry 26*, 1289–1300.

Serpersu, E. H., McCracken, J., Peisach, J., & Mildvan, A. S. (1988) *FASEB J. 2*, Abstract 1696, A588.

Shimizu, T., Mims, W. B., Peisach, J., & Davis, J. L. (1979) *J. Chem. Phys. 70*, 2249–2254.

Slater, J. P., Tamir, I., Loeb, L. A., & Mildvan, A. S. (1972) *J. Biol. Chem. 247*, 6784–6794.

Stezowski, J. J., & Hoard, J. L. (1984) *Isr. J. Chem. 24*, 323–334.

Wells, A. F. (1984) *Structural Inorganic Chemistry*, pp 822–827, Clarendon, Oxford, U.K.

Zweier, J., Aisen, P., Peisach, J., & Mims, W. B. (1979) *J. Biol. Chem. 254*, 3512–3515.